

STABILITY OF THE NON-HERMITIAN SKIN EFFECT

HABIB AMMARI, SILVIO BARANDUN, BRYN DAVIES, ERIK ORVEHED HILTUNEN,
AND PING LIU

ABSTRACT. This paper shows that the skin effect in systems of non-Hermitian sub-wavelength resonators is robust with respect to random imperfections in the system. The subwavelength resonators are highly contrasting material inclusions that resonate in a low-frequency regime. The non-Hermiticity is due to the introduction of an imaginary gauge potential, which leads to a skin effect that is manifested by the system's eigenmodes accumulating at one edge of the structure. We elucidate the topological protection of the associated (real) eigenfrequencies and illustrate the competition between the two different localisation effects present when the system is randomly perturbed: the non-Hermitian skin effect and the disorder-induced Anderson localisation. We show that, as the strength of the disorder increases, more and more eigenmodes become localised in the bulk. Our results are based on an asymptotic matrix model for subwavelength physics and can be generalised also to tight-binding models in condensed matter theory.

Keywords. Non-Hermitian systems, non-Hermitian skin effect, subwavelength resonators, imaginary gauge potential, Toeplitz matrix, eigenvector condensation, Anderson localisation, stability analysis, disorder-induced phase transition.

AMS Subject classifications. 35B34, 47B28, 35P25, 35C20, 81Q12. 15A18, 15B05,

1. Introduction

The skin effect is the phenomenon whereby a large proportion of the bulk eigenmodes of a non-Hermitian system are localised at one edge of an open chain [8, 23]. In subwavelength physics, it emerges in an array of subwavelength resonators when an imaginary gauge potential is introduced inside the resonators, which are much smaller than the operating wavelength. The resonance of these subwavelength structures (whose dimensions are substantially smaller than the operating wavelength) is essential as without exciting the structure's subwavelength resonances the effect of the imaginary gauge potential would be negligible.

In systems of subwavelength resonators, the skin effect phenomenon is unique to non-Hermitian systems with non-reciprocal coupling. While localisation of specific eigenmodes can be achieved in other (*e.g.* Hermitian) systems, the skin effect is characterised by having a large number of the modes (which scales with the size of the system) localised at one edge of the system. This phenomenon has been realised experimentally in both photonic and phononic systems [11, 12, 19, 21, 30, 35]. It significantly advances the field of active metamaterials and opens new avenues to channel and manipulate energy at subwavelength scales [9].

The non-Hermitian skin effect was first introduced in condensed matter physics as a non-Hermitian extension of the Anderson model of localisation [15]. The imaginary gauge potential leads to the simultaneous condensation of an extensive number of bulk eigenmodes, all in the same direction [16, 22, 26, 31]. The tight binding models used in condensed matter theory share many fundamental similarities with the one-dimensional subwavelength classical wave system considered here.

In a recent work [1], the non-Hermitian skin effect in the subwavelength regime was studied using first-principle mathematical analysis. One-dimensional systems of subwavelength resonators were considered, with an imaginary gauge potential added to break Hermiticity.

Explicit asymptotic expressions for the subwavelength eigenfrequencies and eigenmodes were obtained using a gauge capacitance matrix formulation of the problem (which is a reformulation of the standard capacitance matrices that are commonplace in Hermitian subwavelength physics and electrostatics). Moreover, the exponential decay of eigenmodes and their accumulation at one edge of the structure (the non-Hermitian skin effect) was shown to be induced by the Fredholm index of an associated Toeplitz operator. A remaining open question is whether the skin effect is stable with respect to disorder. This important problem has been subject to recent debate in the physics and engineering communities [23].

In this paper, we prove the robustness of the non-Hermitian skin effect with respect to random imperfections in the system. Based on delicate eigenvalue and eigenvector analysis of perturbed “almost-Toeplitz” matrices, we quantify the stability of the non-Hermitian skin effect. Moreover, we illustrate the competition between the non-Hermitian skin effect and Anderson localisation. Anderson localisation here refers to strong localisation of eigenmodes in the bulk (at subwavelength scales) that it is induced by disorder [7]. We observe that, as the disorder strength increases, more and more eigenmodes are localised in the bulk. This leads to a disorder-induced phase transition (in terms of the disorder strength) between accumulation at one edge of the structure and localisation in the bulk. As far as we know, these findings provide the first justification to the experimental results discussed in [18, 20, 27]. It also extends the Anderson localisation in systems of subwavelength resonators [4] to the non-Hermitian case. On the other hand, we also elucidate the topological protection of the (real) eigenfrequencies associated with the eigenmodes that accumulate at one edge of the structure. All of these eigenfrequencies stay inside a region of the complex plane with nontrivial winding number and can, consequently, be said to be topologically protected. Conversely, the eigenfrequencies corresponding to eigenmodes that are localised in the bulk fall outside of this region.

The paper is organised as follows. In Section 2, we present the mathematical setup of the problem and recall its discrete formulation which provides approximations of the eigenfrequencies and eigenmodes of a finite chain of subwavelength resonators in terms of the eigenvalues and eigenvectors of the gauge capacitance matrix. Given this discrete formulation and the effect of uncertainties in the positions of the resonators or their material parameters, we can reduce the stability analysis to the analysis of a perturbed almost-Toeplitz matrices. Section 3 is devoted to the stability analysis of the eigenvalues while in Section 4 we prove the stability of the eigenvectors and show their exponential decay and condensation at one edge of the structure. In Section 5, we numerically illustrate our main findings in this paper. Moreover, we show how condensation of the eigenmodes at the edge and localisation in the bulk are competing effects and present topologically-induced phase transition diagrams in terms of the strength of the disorder. We show numerically that as the strength of the disorder increases, the number of eigenmodes localised in the bulk increases. We also elucidate the fact that the non-trivial winding of the symbol of the associated Toeplitz operator at the eigenfrequencies protects an extensive number of associated eigenmodes from localisation. The paper ends with some concluding remarks and interesting generalisations of the results.

2. Non-Hermitian skin effect

We begin this section by introducing the setting and recalling results from [1] on the non-Hermitian skin effect without disorder. In Section 2.2, we introduce the disordered model which will be studied in subsequent sections.

2.1. Problem formulation

We consider a one-dimensional chain of N disjoint identical subwavelength resonators $D_i := (x_i^L, x_i^R)$, where $(x_i^{L,R})_{1 \leq i \leq N} \subset \mathbb{R}$ are the $2N$ extremities satisfying $x_i^L < x_i^R < x_{i+1}^L$ for any $1 \leq i \leq N$. We fix the coordinates such that $x_1^L = 0$. We also denote by $\ell_i = x_i^R - x_i^L$ the length of each of the resonators, and by $s_i = x_{i+1}^L - x_i^R$ the spacing between the i -th and

$(i + 1)$ -th resonators. The system is illustrated in Figure 2.1. We use

$$D := \bigcup_{i=1}^N (x_i^L, x_i^R)$$

to symbolise the set of subwavelength resonators. In this paper, we only consider systems of equally spaced identical resonators, that is,

$$\ell_i = \ell \in \mathbb{R}_{>0} \text{ for all } 1 \leq i \leq N \quad \text{and} \quad s_i = s \in \mathbb{R}_{>0} \text{ for all } 1 \leq i \leq N - 1.$$

This will simplify the formulas in our subsequent analysis and is sufficient to understand the fundamental mechanisms behind the skin and localisation effects we are interested in.

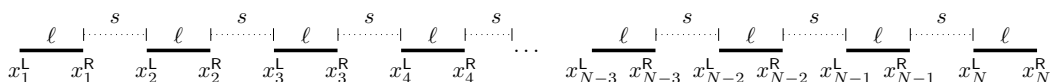


FIGURE 2.1. A chain of N one-dimensional subwavelength resonators, with length ℓ and spacing s .

In this work, we consider the following one-dimensional damped wave equation where the damping acts in the space dimension instead of the time dimension:

$$-\frac{\omega^2}{\kappa(x)}u(x) - \gamma(x)\frac{d}{dx}u(x) - \frac{d}{dx}\left(\frac{1}{\rho(x)}\frac{d}{dx}u(x)\right) = 0, \quad x \in \mathbb{R}, \quad (2.1)$$

for a piecewise constant damping coefficient

$$\gamma(x) = \begin{cases} \gamma, & x \in D, \\ 0, & x \in \mathbb{R} \setminus D. \end{cases} \quad (2.2)$$

The parameter γ extends the usual scalar wave equation to a generalised Strum–Liouville equation via the introduction of an imaginary gauge potential [32]. The material parameters $\kappa(x)$ and $\rho(x)$ are piecewise constant

$$\kappa(x) = \begin{cases} \kappa_b & x \in D, \\ \kappa & x \in \mathbb{R} \setminus D, \end{cases} \quad \text{and} \quad \rho(x) = \begin{cases} \rho_b & x \in D, \\ \rho & x \in \mathbb{R} \setminus D, \end{cases}$$

where the constants $\rho_b, \rho, \kappa, \kappa_b \in \mathbb{R}_{>0}$. The wave speeds inside the resonators D and inside the background medium $\mathbb{R} \setminus D$, are denoted respectively by v_b and v , the wave numbers respectively by k_b and k , the frequency by ω , and the contrast between the densities of the resonators and the background medium by δ :

$$v_b := \sqrt{\frac{\kappa_b}{\rho_b}}, \quad v := \sqrt{\frac{\kappa}{\rho}}, \quad k_b := \frac{\omega}{v_b}, \quad k := \frac{\omega}{v}, \quad \delta := \frac{\rho_b}{\rho}. \quad (2.3)$$

We are interested in the resonances $\omega \in \mathbb{C}$ such that (2.1) has a non-trivial solution in a high-contrast, low-frequency (subwavelength) regime. This regime is typically characterised by letting the contrast parameter $\delta \rightarrow 0$ and looking for solutions which are such that $\omega \rightarrow 0$ as $\delta \rightarrow 0$. One consequence of this asymptotic ansatz is that it lends itself to characterisation using asymptotic analysis [5]. Note that this limit recovers subwavelength resonances, while keeping the size of the resonators fixed.

In [1], an asymptotic analysis in the subwavelength limit was performed on the system of non-Hermitian one-dimensional subwavelength resonators considered here. It was shown that the resonances are given by the eigenstates of the *gauge capacitance matrix* \mathcal{C}^γ . This is a modified version of the conventional capacitance matrix that is often used to characterise many-body low-frequency resonance problems; see, for instance, [5].

The following results are from [1].

Theorem 2.1. *Let the gauge capacitance matrix $\mathcal{C}^\gamma = (\mathcal{C}_{i,j}^\gamma)_{i,j=1}^N$ be defined by*

$$\mathcal{C}_{i,j}^\gamma := \begin{cases} \frac{\gamma}{s} \frac{1}{1 - e^{-\gamma\ell}}, & i = j = 1, \\ \frac{\gamma}{s} \coth(\gamma\ell/2), & 1 < i = j < N, \\ \pm \frac{\gamma}{s} \frac{1}{1 - e^{\pm\gamma}}, & 1 \leq i = j \pm 1 \leq N, \\ -\frac{\gamma}{s} \frac{1}{1 - e^{\gamma\ell}}, & i = j = N. \end{cases} \quad (2.4)$$

Then,

(i) *All the eigenvalues of \mathcal{C}^γ are real. They are given by*

$$\begin{aligned} \lambda_1 &= 0, \\ \lambda_k &= \frac{\gamma}{s} \coth(\gamma\ell/2) + \frac{2|\gamma|}{s} \frac{e^{\frac{\gamma\ell}{2}}}{|e^{\gamma\ell} - 1|} \cos\left(\frac{\pi}{N}k\right), \quad 2 \leq k \leq N. \end{aligned} \quad (2.5)$$

Furthermore, the associated eigenvectors \mathbf{a}_k satisfy the following inequality, for $2 \leq k \leq N$

$$|\mathbf{a}_k^{(i)}| \leq \kappa_k e^{-\gamma\ell \frac{i-1}{2}} \quad \text{for all } 1 \leq i \leq N, \quad (2.6)$$

for some $\kappa_k \leq (1 + e^{\frac{\gamma\ell}{2}})^2$. Here, $\mathbf{a}_k^{(i)}$ denotes the i -th entry of the eigenvector \mathbf{a}_k ;

(ii) *The N subwavelength eigenfrequencies ω_i of (2.1) satisfy, as $\delta \rightarrow 0$,*

$$\omega_i = v_b \sqrt{\delta \lambda_i} + \mathcal{O}(\delta),$$

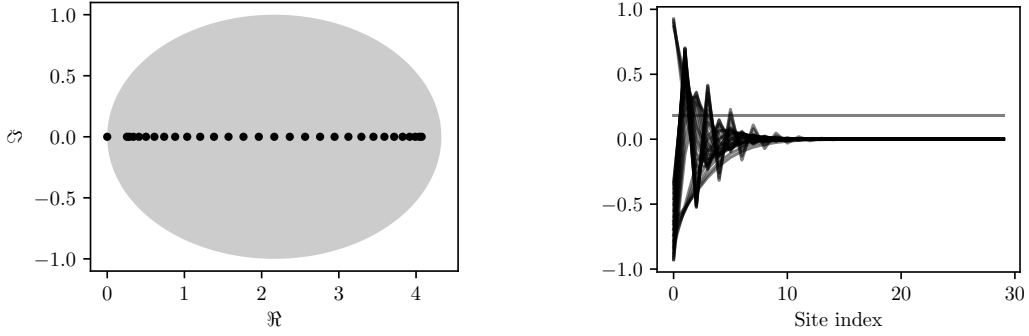
where $(\lambda_i)_{1 \leq i \leq N}$ are the eigenvalues of \mathcal{C}^γ . Furthermore, let u_i be a subwavelength eigenmode corresponding to ω_i and let \mathbf{a}_i be the corresponding eigenvector of \mathcal{C}^γ . Then

$$u_i(x) = \sum_j \mathbf{a}_i^{(j)} V_j(x) + \mathcal{O}(\delta),$$

where V_j are defined by

$$\begin{cases} -\frac{d^2}{dx^2} V_i = 0, & x \in \mathbb{R} \setminus \bigcup_{i=1}^N (x_i^L, x_i^R), \\ V_i(x) = \delta_{ij}, & x \in (x_j^L, x_j^R), \\ V_i(x) = \mathcal{O}(1) & \text{as } |x| \rightarrow \infty. \end{cases} \quad (2.7)$$

From Theorem 2.1, we can see that \mathcal{C}^γ is *almost* Toeplitz (in the sense that it has constant diagonals other than deterministic perturbations in the corners) and its eigenvectors display exponential decay both with respect to the site index i and the factor γ . This shows the condensation of bulk eigenmodes at one of the edges of the system of subwavelength resonators. The exponential decay of the eigenvectors is directly linked with a topological property. Let T be a Toeplitz operator with continuous symbol f_T and T_N be the truncation of T to the upper-left $N \times N$ submatrix. Then, if f_T is sufficiently smooth, standard Toeplitz theory says that any eigenvalue $\lambda \in \mathbb{C}$ which is such that the winding $w(f_T, \lambda)$ of f_T at λ is negative will be such that the corresponding eigenvector decays exponentially. We show this topological region in Figure 2.2a for our system. In Figure 2.2b we plot the eigenvectors superimposed on one another to portray condensation on the left edge of the structure; $\lambda_1 = 0$ corresponds to a trivial (constant) eigenvector while all other eigenvectors are exponentially localised to the left edge of the structure.



- (A) Shaded in grey is the region where the symbol f_T has negative winding, for T the Toeplitz operator corresponding to the capacitance matrix \mathcal{C}^γ . The black dots show the spectrum of \mathcal{C}^γ .
- (B) Eigenvector condensation on the left edge of the structure. The 30 modes are plotted, superimposed. The constant eigenvector is the one associated to the eigenvalue 0.

FIGURE 2.2. Numerical simulations for an unperturbed system of $N = 30$ resonators with $s = \ell = 1$ and $\gamma = 1$.

2.2. Randomly perturbed gauge capacitance matrix

To simplify the notation, we denote the tridiagonal Toeplitz matrix with deterministic perturbations on diagonal corners by

$$T_N^{(a,b)} = \begin{pmatrix} \alpha + a & \beta & 0 & 0 & \dots & 0 & 0 \\ \eta & \alpha & \beta & 0 & \dots & 0 & 0 \\ 0 & \eta & \alpha & \beta & \dots & 0 & 0 \\ \dots & \dots & \dots & \dots & \dots & \dots & \dots \\ \dots & \dots & \dots & \dots & \dots & \alpha & \beta \\ 0 & 0 & 0 & 0 & \dots & \eta & \alpha + b \end{pmatrix}. \quad (2.8)$$

Throughout the paper, we only consider $T_N^{(a,b)}$ with $\alpha, \eta, \beta, a, b \in \mathbb{R}$ and $\eta\beta > 0$. In particular, observe from (2.4) that

$$\mathcal{C}^\gamma = T_N^{(\eta,\beta)}$$

and η, α, β are such that

$$a = \eta, \quad b = \beta, \quad \eta\beta > 0 \quad \text{and,} \quad \eta + \alpha + \beta = 0.$$

Note also that $T_N^{(0,0)}$ is a tridiagonal Toeplitz matrix.

In order to study the stability of the non-Hermitian skin effect with respect to random imperfections in the system design, we either add random errors to the positions of the resonators (keeping the length of the resonators unchanged) or to the γ -term and then repeatedly compute the subwavelength eigenfrequencies and eigenmodes. The perturbations in the positions and in the values of the γ -parameter are drawn at random from uniform distributions with zero-mean values. Since these random perturbations affect only the tridiagonal entries of the gauge capacitance matrix $\widehat{\mathcal{C}}^\gamma$ of the randomly perturbed system, we can write in both cases that

$$\widehat{\mathcal{C}}^\gamma = \widehat{T}_N^{(a,b)} := \begin{pmatrix} \alpha + a + \varepsilon_{\alpha,1} & \beta + \varepsilon_{\beta,1} & 0 & \dots & 0 & 0 \\ \eta + \varepsilon_{\eta,2} & \alpha + \varepsilon_{\alpha,2} & \beta + \varepsilon_{\beta,2} & \dots & 0 & 0 \\ 0 & \eta + \varepsilon_{\eta,3} & \alpha + \varepsilon_{\alpha,3} & \dots & 0 & 0 \\ \dots & \dots & \dots & \dots & \dots & \dots \\ \dots & \dots & \dots & \dots & \alpha + \varepsilon_{\alpha,N-1} & \beta + \varepsilon_{\beta,N-1} \\ 0 & 0 & 0 & \dots & \eta + \varepsilon_{\eta,N} & \alpha + b + \varepsilon_{\alpha,N} \end{pmatrix} \quad (2.9)$$

with $a = \eta, b = \beta$.

3. Stability of eigenvalues

In this section, we derive stability results for the eigenvalues of $T_N^{(a,b)}$. This relies on a crucial observation that the tridiagonal matrix $T_N^{(a,b)}$ always has same eigenvalues as a Hermitian matrix. Thus we first recall the following well known Weyl theorem for the stability of eigenvalues of Hermitian matrices; see [25, Theorem 1.1.7], [13, Theorem 8.1.6] and [24, Theorem 10.3.1]. We also refer the reader to [17] for some more refined results.

Theorem 3.1. *Let A and E be $N \times N$ Hermitian matrices. For $k \in \{1, \dots, N\}$ denote by $\lambda_k(A + E), \lambda_k(A)$ the k -th eigenvalue of $A + E$ and A , respectively. Assume these to be arranged in a decreasing sequence. Then*

$$|\lambda_k(A + E) - \lambda_k(A)| \leq \|E\|_2.$$

We next recall the following result [1, Lemma A.6] on the eigenvalues of $T_N^{(\eta,\beta)}$ where its proof comes from [34].

LEMMA 3.2. *Suppose that $\eta + \alpha + \beta = 0$. Let λ be an eigenvalue of $T_N^{(\eta,\beta)}$. Then, either $\lambda = \lambda_1 := 0$ and the corresponding eigenvector is $\mathbf{x}_1 = \mathbf{1}$ or*

$$\lambda_k := \alpha + 2\sqrt{\eta\beta} \cos\left(\frac{\pi}{N}(k-1)\right), \quad 2 \leq k \leq N, \quad (3.1)$$

and the corresponding eigenvector is \mathbf{x}_k , with entries

$$\mathbf{x}_k^{(j)} = \left(\frac{\eta}{\beta}\right)^{\frac{j-1}{2}} \left(\eta \sin\left(\frac{j(k-1)\pi}{N}\right) - \eta\sqrt{\frac{\eta}{\beta}} \sin\left(\frac{(j-1)(k-1)\pi}{N}\right) \right), \quad j = 1, \dots, N. \quad (3.2)$$

Then we state our result on the stability of the eigenvalues of $T_N^{(a,b)}$ with $a, b \in \mathbb{R}$.

Theorem 3.3. *The eigenvalues of $T_N^{(a,b)}$ and $\widehat{T}_N^{(a,b)}$ are all real numbers. Let $\{\lambda_k\}, \{\widehat{\lambda}_k\}$ be respectively the eigenvalues of $T_N^{(a,b)}$ and $\widehat{T}_N^{(a,b)}$, arranged in decreasing sequences. Assuming that*

$$\max_{j=1, \dots, N} (|\varepsilon_{\eta,j}|, |\varepsilon_{\alpha,j}|, |\varepsilon_{\beta,j}|) =: \varepsilon, \quad (3.3)$$

then we have

$$\left| \widehat{\lambda}_k - \lambda_k \right| < C_1(\eta, \beta, \varepsilon)\varepsilon,$$

where

$$C_1(\eta, \beta, \varepsilon) = \frac{|\beta| + |\eta| + \varepsilon}{\sqrt{\beta\eta}} + 1. \quad (3.4)$$

Proof. Note that all the λ_k 's are real since $T_N^{(a,b)}$ has the same eigenvalues as the Hermitian matrix

$$A = \begin{pmatrix} \alpha + a & \sqrt{\eta\beta} & 0 & 0 & \dots & 0 & 0 \\ \sqrt{\eta\beta} & \alpha & \sqrt{\eta\beta} & 0 & \dots & 0 & 0 \\ 0 & \sqrt{\eta\beta} & \alpha & \sqrt{\eta\beta} & \dots & 0 & 0 \\ \dots & \dots & \dots & \dots & \dots & \dots & \dots \\ \dots & \dots & \dots & \dots & \dots & \alpha & \sqrt{\eta\beta} \\ 0 & 0 & 0 & 0 & \dots & \sqrt{\eta\beta} & \alpha + b \end{pmatrix} \quad (3.5)$$

which can be seen from $|xI - T_N^{(a,b)}| = |xI - A|$ by expanding the determinant along the last row. Here, $|\cdot|$ denotes the determinant. In the same manner, all the $\widehat{\lambda}_k$'s are real, as

$\widehat{T}_N^{(a,b)}$ has the same eigenvalues as the Hermitian matrix

$$\widetilde{T}_N^{(a,b)} = \begin{pmatrix} \alpha + a + \varepsilon_{\alpha,1} & x_{1,2} & 0 & 0 & \dots & 0 & 0 \\ & x_{2,1} & \alpha + \varepsilon_{\alpha,2} & x_{2,3} & 0 & \dots & 0 & 0 \\ & 0 & x_{3,2} & \alpha + \varepsilon_{\alpha,3} & x_{3,4} & \dots & 0 & 0 \\ \dots & \dots & \dots & \dots & \dots & \dots & \dots & \dots \\ \dots & \dots & \dots & \dots & \dots & \dots & \alpha + \varepsilon_{\alpha,N-1} & x_{N-1,N} \\ & 0 & 0 & 0 & 0 & \dots & x_{N,N-1} & \alpha + b + \varepsilon_{\alpha,n} \end{pmatrix},$$

where

$$x_{j,j+1} = x_{j+1,j} = \sqrt{(\beta + \varepsilon_{\beta,j})(\eta + \varepsilon_{\eta,j+1})}, \quad j = 1, \dots, N-1.$$

Now, we can make use of Theorem 3.1 to analyse the stability of the eigenvalues of A . Let

$$\widetilde{\varepsilon}_{j,j+1} = \widetilde{\varepsilon}_{j+1,j} = \sqrt{(\beta + \varepsilon_{\beta,j})(\eta + \varepsilon_{\eta,j+1})} - \sqrt{\beta\eta}, \quad j = 1, \dots, N-1,$$

and

$$\widetilde{\varepsilon}_{j,j} = \varepsilon_{\alpha,j}, \quad j = 1, \dots, N.$$

It is not hard to see that

$$|\widetilde{\varepsilon}_{j,j+1}| < \left(\frac{|\beta| + |\eta| + \varepsilon}{2\sqrt{\beta\eta}} \right) \varepsilon, \quad j = 1, \dots, N-1,$$

as $\varepsilon \leq 1$. We decompose $\widetilde{T}_N^{(a,b)}$ as

$$A + E,$$

where $E_{i,j} = \widetilde{\varepsilon}_{i,j}$, for $i = j, i = j+1, i = j-1$, and $E_{i,j} = 0$ for other i, j . In particular, the following estimate holds:

$$\|E\|_2 = \max_{\|v\|_2=1} \|Ev\|_2 < \left(\frac{|\beta| + |\eta| + \varepsilon}{\sqrt{\beta\eta}} + 1 \right) \varepsilon.$$

The above estimate can be derived from the fact that

$$\begin{aligned} Ev &= \begin{pmatrix} \widetilde{\varepsilon}_{1,1}v_1 + \widetilde{\varepsilon}_{1,2}v_2 \\ \widetilde{\varepsilon}_{2,1}v_1 + \widetilde{\varepsilon}_{2,2}v_2 + \widetilde{\varepsilon}_{2,3}v_3 \\ \vdots \\ \widetilde{\varepsilon}_{N-1,N-2}v_{N-2} + \widetilde{\varepsilon}_{N-1,N-1}v_{N-1} + \widetilde{\varepsilon}_{N-1,N}v_N \\ \widetilde{\varepsilon}_{N,N-1}v_{N-1} + \widetilde{\varepsilon}_{N,N}v_N \end{pmatrix} \\ &= \begin{pmatrix} 0 \\ \widetilde{\varepsilon}_{2,1}v_1 \\ \vdots \\ \widetilde{\varepsilon}_{N-1,N-2}v_{N-2} \\ \widetilde{\varepsilon}_{N,N-1}v_{N-1} \end{pmatrix} + \begin{pmatrix} \widetilde{\varepsilon}_{1,1}v_1 \\ \widetilde{\varepsilon}_{2,2}v_2 \\ \vdots \\ \widetilde{\varepsilon}_{N-1,N-1}v_{N-1} \\ \widetilde{\varepsilon}_{N,N}v_N \end{pmatrix} + \begin{pmatrix} \widetilde{\varepsilon}_{1,2}v_2 \\ \widetilde{\varepsilon}_{2,3}v_3 \\ \vdots \\ \widetilde{\varepsilon}_{N-1,N}v_N \\ 0 \end{pmatrix}, \end{aligned}$$

where $v = (v_1, \dots, v_N)^\top$ with the superscript \top denoting the transpose.

Leveraging Theorem 3.1 then proves the statement. \blacksquare

REMARK 3.4. Due to the fact that the matrix $T_N^{(a,b)}$ is tridiagonal and the Hermitian matrix A is stable, we do not require any constraint on the perturbation level in Theorem 3.3. When it comes to banded Toeplitz matrices and complex perturbations, the findings and proofs are more intricate. We refer the readers to [28, 29] for further information on this subject.

Applying Theorem 3.3 to the eigenvalues of $T_N^{(\eta,\beta)}$ in Lemma 3.2 yields the following stability estimate.

Theorem 3.5. For the eigenvalue $\widehat{\lambda}_k$ of the perturbed Toeplitz matrix $\widehat{T}_N^{(\eta,\beta)}$ with

$$\max_{j=1,\dots,N} (|\varepsilon_{\eta,j}|, |\varepsilon_{\alpha,j}|, |\varepsilon_{\beta,j}|) =: \varepsilon, \quad (3.6)$$

we have $\widehat{\lambda}_1 = \varepsilon_1$ and

$$\widehat{\lambda}_k = \lambda_k + \varepsilon_k = \alpha + 2\sqrt{\eta\beta} \cos\left(\frac{(k-1)\pi}{N}\right) + \varepsilon_k, \quad k = 2, \dots, N, \quad (3.7)$$

with $|\varepsilon_k| \leq C_1(\eta, \beta, \varepsilon)\varepsilon$, $1 \leq k \leq N$ and $C_1(\eta, \beta, \varepsilon)$ being defined by (3.4). In particular, all the $\widehat{\lambda}_k$'s are real numbers.

REMARK 3.6. The eigenvalues of the tridiagonal Toeplitz matrix $T_N^{(0,0)}$ have been proved [10, 14] to be

$$\lambda_k = \alpha + 2\sqrt{\eta\beta} \cos\left(\frac{k\pi}{N+1}\right), \quad k = 1, \dots, N.$$

REMARK 3.7. One can apply Theorems 3.3 and 4.1 to derive similar stability results for $T_N^{(0,0)}$. This corresponds to many examples in the non-Hermitian skin effect in condensed matter theory and quantum mechanics and thus our stability results here can be immediately applied to those examples. For the eigenvalues of the tridiagonal Toeplitz matrix with various perturbations on the corners, we refer the reader to [33, 34].

4. Stability of eigenvectors

This section is devoted to estimating the stability of the eigenvectors of $\mathcal{C}^\gamma = T_N^{(\eta,\beta)}$.

For λ_k defined in (3.1), let

$$p_j(\lambda_k) = \left(\eta \sin\left(\frac{(j+1)(k-1)\pi}{N}\right) - \eta\sqrt{\frac{\eta}{\beta}} \sin\left(\frac{j(k-1)\pi}{N}\right) \right), \quad j = 0, \dots, N-1. \quad (4.1)$$

Note that

$$|p_j(\lambda_k)| \leq |\eta| \left(1 + \sqrt{\frac{\eta}{\beta}} \right), \quad j = 0, \dots, N-1. \quad (4.2)$$

The following results hold.

Theorem 4.1. For $\widehat{T}_N^{(\eta,\beta)}$ defined by (2.9) and satisfying (3.6) and its eigenvalues $\widehat{\lambda}_k = \lambda_k + \varepsilon_k$, $k = 2, \dots, N$ defined by (3.7), the corresponding eigenvectors are given by

$$\begin{aligned} \widehat{\mathbf{x}}_k = & (p_0(\lambda_k) + \delta_0(\lambda_k), s(p_1(\lambda_k) + \delta_1(\lambda_k)), s^2(p_2(\lambda_k) + \delta_2(\lambda_k)), \dots, \\ & s^{N-1}(p_{N-1}(\lambda_k) + \delta_{N-1}(\lambda_k)))^\top, \quad k = 2, \dots, N, \end{aligned} \quad (4.3)$$

where $s = \sqrt{\frac{\eta}{\beta}}$ and $p_j(\lambda_k)$ is defined in (4.1). Moreover, we have

$$|(-s)^j p_j(\lambda_k)| \leq \left(\frac{\eta}{\beta}\right)^{\frac{j}{2}} |\eta| \left(1 + \sqrt{\frac{\eta}{\beta}} \right), \quad j = 0, 1, \dots, N-1, \quad (4.4)$$

and

$$|s^j \delta_j(\lambda_k)| \leq \zeta_{k,j} \varepsilon, \quad j = 0, 1, \dots, N-1, \quad (4.5)$$

where

$$\zeta_{k,j} = \left(\sqrt{\frac{\eta}{\beta}} \left(\frac{|\beta|(|\eta| + \varepsilon)}{(|\beta| - \varepsilon)|\eta|} \right) \right)^j (a_+ r_{k,+}^j + a_- r_{k,-}^j - \zeta)$$

with

$$r_{k,\pm} = \left(\left| \cos\left(\frac{(k-1)\pi}{N}\right) \right| + \frac{C_2(\eta, \beta)\varepsilon}{\sqrt{\eta\beta}} \right) \pm \sqrt{\left(\left| \cos\left(\frac{(k-1)\pi}{N}\right) \right| + \frac{C_2(\eta, \beta)\varepsilon}{\sqrt{\eta\beta}} \right)^2 + 1}, \quad (4.6)$$

$C_2(\eta, \beta, \varepsilon) = \frac{|\beta| + |\eta| + \varepsilon}{2\sqrt{\beta\eta}} + 1$, and a_+, a_-, ζ being bounded constants. In particular, for those indices k such that

$$\left| \sqrt{\frac{\eta}{\beta}} \left(\frac{|\beta|(|\eta| + \varepsilon)}{(|\beta| - \varepsilon)|\eta|} \right) r_{k,+} \right| < 1, \quad (4.7)$$

the corresponding eigenvector still has an exponential decay.

As a result, there exists a constant c such that if $\sqrt{\eta/\beta} < \sqrt{2} - 1$ and $\varepsilon < \frac{c}{N^2}$, then we still have exponential decay for all the corresponding eigenvectors $\widehat{\mathbf{x}}_k$, $2 \leq k \leq N$, of $\widehat{T}_N^{(a,b)}$. Further, if we require $\sqrt{\eta/\beta}$ to be even smaller, then this exponential decay will remain for even larger values of ε .

Proof. The inequality (4.4) is a direct consequence of (3.2) and (4.2). The rest of the argument consists in proving (4.5). For fixed λ_k , we see that

$$|\delta_j(\lambda_k)| \leq \left(\frac{|\beta|(|\eta| + \varepsilon)}{(|\beta| - \varepsilon)|\eta|} \right)^j M_j \varepsilon \quad (4.8)$$

and will analyse the constants M_j . We consider the eigenvalue problem

$$\left(\widehat{T}_N^{(\eta,\beta)} - \widehat{\lambda}_k I \right) \widehat{\mathbf{x}}_k = 0, \quad (4.9)$$

where $\widehat{\mathbf{x}}_k$ is (4.3). For simplicity, we abbreviate $p_j(\lambda_k)$ as p_j and $\delta_j(\lambda_k)$ as δ_j in the proof. Based on the first row in (4.9), we have

$$(\alpha + \eta + \varepsilon_{\alpha,1} - \lambda_k - \varepsilon_k)(p_0 + \delta_0) + (\beta + \varepsilon_{\beta,1})s(p_1 + \delta_1) = 0.$$

This gives

$$(\varepsilon_{\alpha,1} - \varepsilon_k)p_0 + \varepsilon_{\beta,1}sp_1 + (\alpha + \eta + \varepsilon_{\alpha,1} - \lambda_k - \varepsilon_k)\delta_0 + (\beta + \varepsilon_{\beta,1})s\delta_1 = 0,$$

where we have used $(\alpha + \eta - \lambda_k)p_0 + \beta sp_1 = 0$. Let $\delta_0 = \varepsilon$. Then

$$M_0 = 1$$

and

$$\delta_1 = \frac{(\varepsilon_{\alpha,1} - \varepsilon_k)p_0 + \varepsilon_{\beta,1}sp_1 + (\alpha + \eta + \varepsilon_{\alpha,1} - \lambda_k - \varepsilon_k)\varepsilon}{-(\beta + \varepsilon_{\beta,1})s}.$$

Denote $C_2(\eta, \beta, \varepsilon) = \frac{|\beta| + |\eta| + \varepsilon}{2\sqrt{\beta\eta}} + 1$. Then we have

$$\begin{aligned} |\delta_1| &\leq \left| \frac{(\varepsilon_{\alpha,1} - \varepsilon_k)p_0 + \varepsilon_{\beta,1}sp_1}{-(\beta + \varepsilon_{\beta,1})s} \right| + \left| \frac{(\alpha + \eta + \varepsilon_{\alpha,1} - \lambda_k - \varepsilon_k)\varepsilon}{-(\beta + \varepsilon_{\beta,1})s} \right| \\ &\leq \frac{|\eta|(1+s)(2C_2(\eta, \beta) + s)\varepsilon}{(|\beta| - \varepsilon)s} + \frac{|\eta| + 2\sqrt{\eta\beta} \left| \cos\left(\frac{(k-1)\pi}{N}\right) \right| + 2C_2(\eta, \beta, \varepsilon)\varepsilon}{(|\beta| - \varepsilon)s} \\ &\leq \left(\frac{|\beta|(|\eta| + \varepsilon)}{(|\beta| - \varepsilon)|\eta|} \right) \left(s(1+s)(2C_2(\eta, \beta, \varepsilon) + s) + s + 2 \left| \cos\left(\frac{(k-1)\pi}{N}\right) \right| + \frac{2C_2(\eta, \beta, \varepsilon)\varepsilon}{\sqrt{\eta\beta}} \right) \varepsilon, \end{aligned}$$

where we have used (4.2) and Theorem 3.5 in the second inequality. Therefore,

$$M_1 = s(1+s)(2C_2(\eta, \beta, \varepsilon) + s) + s + 2 \left| \cos\left(\frac{(k-1)\pi}{N}\right) \right| + \frac{2C_2(\eta, \beta, \varepsilon)\varepsilon}{\sqrt{\eta\beta}}.$$

We now analyse the relation between M_{j-1} , M_j and M_{j+1} . Based on the $(j+1)$ -th row of (4.9), we have

$$(\eta + \varepsilon_{\eta,j+1})s^{j-1}(p_{j-1} + \delta_{j-1}) + (\alpha + \varepsilon_{\alpha,j+1} - \lambda_k - \varepsilon_k)s^j(p_j + \delta_j) + (\beta + \varepsilon_{\beta,j+1})s^{j+1}(p_{j+1} + \delta_{j+1}) = 0,$$

which yields

$$(\eta + \varepsilon_{\eta,j+1})(p_{j-1} + \delta_{j-1}) + (\alpha + \varepsilon_{\alpha,j+1} - \lambda_k - \varepsilon_k)s(p_j + \delta_j) + (\beta + \varepsilon_{\beta,j+1})s^2(p_{j+1} + \delta_{j+1}) = 0.$$

Making use of the identity

$$\eta p_{j-1} + (\alpha - \lambda_k)sp_j + \beta s^2 p_{j+1} = 0,$$

we can eliminate some items to arrive at

$$\begin{aligned} \varepsilon_{\eta,j+1}p_{j-1} + (\varepsilon_{\alpha,j+1} - \varepsilon_k)sp_j + \varepsilon_{\beta,j+1}s^2 p_{j+1} \\ + (\eta + \varepsilon_{\eta,j+1})\delta_{j-1} + (\alpha + \varepsilon_{\alpha,j+1} - \lambda_k - \varepsilon_k)s\delta_j + (\beta + \varepsilon_{\beta,j+1})s^2\delta_{j+1} = 0. \end{aligned}$$

Therefore,

$$\begin{aligned}
 & \delta_{j+1} \\
 &= \frac{\varepsilon_{\eta,j+1} p_{j-1} + (\varepsilon_{\alpha,j+1} - \varepsilon_k) s p_j + \varepsilon_{\beta,j+1} s^2 p_{j+1} + (\eta + \varepsilon_{\eta,j+1}) \delta_{j-1} + (\alpha + \varepsilon_{\alpha,j+1} - \lambda_k - \varepsilon_k) s \delta_j}{-(\beta + \varepsilon_{\beta,j+1}) s^2} \\
 &= \frac{\varepsilon_{\eta,j+1} p_{j-1} + (\varepsilon_{\alpha,j+1} - \varepsilon_k) s p_j + \varepsilon_{\beta,j+1} s^2 p_{j+1}}{-(\beta + \varepsilon_{\beta,j+1}) s^2} \\
 &\quad + \frac{(\eta + \varepsilon_{\eta,j+1}) \delta_{j-1}}{-(\beta + \varepsilon_{\beta,j+1}) s^2} + \frac{(\alpha + \varepsilon_{\alpha,j+1} - \lambda_k - \varepsilon_k) s \delta_j}{-(\beta + \varepsilon_{\beta,j+1}) s^2} \\
 &:= I_1 + I_2 + I_3.
 \end{aligned}$$

For the term I_1 , by (4.2) we have

$$\begin{aligned}
 & \left| \frac{\varepsilon_{\eta,j+1} p_{j-1} - (\varepsilon_{\alpha,j+1} - \varepsilon_k) s p_j + \varepsilon_{\beta,j+1} s^2 p_{j+1}}{-(\beta + \varepsilon_{\beta,j+1}) s^2} \right| \leq \frac{\varepsilon(1 + 2C_2(\eta, \beta, \varepsilon)s + s^2) |\eta| (1 + s)}{(|\beta| - \varepsilon) s^2} \\
 & \leq \frac{|\beta|}{|\beta| - \varepsilon} (1 + 2C_2(\eta, \beta, \varepsilon)s + s^2) (1 + s) \varepsilon =: \frac{|\beta|}{|\beta| - \varepsilon} C_3(\eta, \beta, \varepsilon) \varepsilon.
 \end{aligned}$$

For the term I_2 , by (4.8) we obtain that

$$\left| \frac{(\eta + \varepsilon_{\eta,j+1}) \delta_{j-1}}{-(\beta + \varepsilon_{\beta,j+1}) s^2} \right| \leq \frac{|\eta| + \varepsilon}{(|\beta| - \varepsilon) s^2} \left(\frac{|\beta| (|\eta| + \varepsilon)}{(|\beta| - \varepsilon) |\eta|} \right)^{j-1} M_{j-1} \varepsilon \leq \left(\frac{|\beta| (|\eta| + \varepsilon)}{(|\beta| - \varepsilon) |\eta|} \right)^{j+1} M_{j-1} \varepsilon.$$

For the term I_3 , by Theorem 3.5 and estimate (4.8), it follows that

$$\begin{aligned}
 & \left| \frac{(\alpha + \varepsilon_{\alpha,j+1} - \lambda_k - \varepsilon_k) s \delta_j}{-(\beta + \varepsilon_{\beta,j+1}) s^2} \right| \leq \frac{2\sqrt{\eta\beta} \left| \cos \left(\frac{(k-1)\pi}{N} \right) \right| + 2C_2(\eta, \beta, \varepsilon) \varepsilon}{(|\beta| - \varepsilon) s} |\delta_j| \\
 & \leq \frac{|\beta|}{|\beta| - \varepsilon} \left(2 \left| \cos \left(\frac{(k-1)\pi}{N} \right) \right| + \frac{2C_2(\eta, \beta, \varepsilon) \varepsilon}{\sqrt{\eta\beta}} \right) \left(\frac{|\beta| (|\eta| + \varepsilon)}{(|\beta| - \varepsilon) |\eta|} \right)^j M_j \varepsilon.
 \end{aligned}$$

Therefore, we have

$$|\delta_{j+1}| \leq \left(\frac{|\beta| (|\eta| + \varepsilon)}{(|\beta| - \varepsilon) |\eta|} \right)^{j+1} \left(2 \left(\left| \cos \left(\frac{(k-1)\pi}{N} \right) \right| + \frac{C_2(\eta, \beta, \varepsilon) \varepsilon}{\sqrt{\eta\beta}} \right) M_j + M_{j-1} + C_3(\eta, \beta, \varepsilon) \right) \varepsilon.$$

By (4.8), the recurrence relation is

$$M_{j+1} = 2 \left(\left| \cos \left(\frac{(k-1)\pi}{N} \right) \right| + \frac{C_2(\eta, \beta, \varepsilon) \varepsilon}{\sqrt{\eta\beta}} \right) M_j + M_{j-1} + C_3(\eta, \beta, \varepsilon). \quad (4.10)$$

Define

$$\widetilde{M}_j = M_j + \zeta \quad (4.11)$$

with

$$\zeta = \frac{C_3(\eta, \beta, \varepsilon)}{2 \left(\left| \cos \left(\frac{(k-1)\pi}{N} \right) \right| + \frac{C_2(\eta, \beta, \varepsilon) \varepsilon}{\sqrt{\eta\beta}} \right)}.$$

Then (4.10) yields

$$\widetilde{M}_{j+1} = 2 \left(\left| \cos \left(\frac{(k-1)\pi}{N} \right) \right| + \frac{C_2(\eta, \beta, \varepsilon) \varepsilon}{\sqrt{\eta\beta}} \right) \widetilde{M}_j + \widetilde{M}_{j-1}.$$

This is a linear recurrence relation. To solve it, we consider the roots of its characteristic equation

$$r_k^2 = 2 \left(\left| \cos \left(\frac{(k-1)\pi}{N} \right) \right| + \frac{C_2(\eta, \beta, \varepsilon) \varepsilon}{\sqrt{\eta\beta}} \right) r_k + 1,$$

which are given by (4.6). Thus we have

$$\widetilde{M}_j = a_+ r_{k,+}^j + a_- r_{k,-}^j,$$

with a_+, a_- being chosen to satisfy the initial conditions

$$\widetilde{M}_0 = M_0 + \zeta, \widetilde{M}_1 = M_1 + \zeta.$$

It is not hard to see that a_+, a_- are bounded. Now, by (4.11), M_j reads

$$M_j = a_+ r_{k,+}^j + a_- r_{k,-}^j - \zeta,$$

and we thus have

$$|\delta_j| \leq \left(\frac{|\beta| (|\eta| + \varepsilon)}{(|\beta| - \varepsilon)|\eta|} \right)^j \left(a_+ r_{k,+}^j + a_- r_{k,-}^j - \zeta \right) \varepsilon.$$

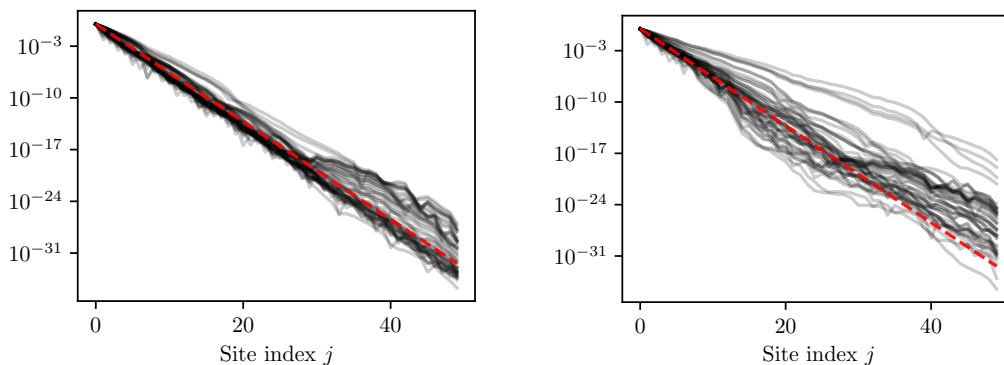
This proves (4.5). ■

Some remarks are now in order.

REMARK 4.2. The stability results obtained in Sections 3 and 4 can be generalised to the dimer case where one can utilise the characterization of the eigenvalues and eigenvectors given in [3].

REMARK 4.3. Note that the perturbation to the spacings $\{s_i\}$ between subwavelength resonators or the coefficient γ in (2.2) of order ε will result in an $O(\varepsilon)$ perturbation in the nonzero entries of the gauge capacitance matrix \mathcal{C}^γ . Thus, Theorem 4.1 can be applied to $\widehat{\mathcal{C}}^\gamma$ to obtain a stability estimate to the eigenvectors and the skin effect of \mathcal{C}^γ .

We can illustrate numerically the results stated in Theorem 4.1. In particular, we consider typical values in physical applications. We let $\eta = 0.15$, $\beta = 3.15$ (which correspond to $\ell = s = 1$ and $\gamma = 3$) and ε satisfying (4.7). The results are presented in Figure 4.1, where we show the eigenvectors of a system of 50 subwavelength resonators on a logarithmic axis. If the perturbations are sufficiently small that the condition (4.7) is satisfied, then the eigenvectors still all have the $(\sqrt{\beta/\eta})$ decay rate. However, when the perturbations are large enough that condition (4.7) does not hold for some indices, then the corresponding modes have a much lower decay rate.



- (A) Exponential decay of the eigenvectors for ε satisfying (4.7). The eigenvectors superimposed on one another on a semi-log plot. The red dashed line represents $(\sqrt{\beta/\eta})^j$. We observe the same decay rate as the unperturbed case.
- (B) Decay of the eigenvectors for ε *not* satisfying (4.7). The eigenvectors superimposed on one another on a semi-log plot. The red dashed line represents $(\sqrt{\beta/\eta})^j$. We observe several eigenvectors with lower decay rate than the one in Figure 4.1a.

FIGURE 4.1. Numerical illustration of the stability of the eigenvector decay rate predicted by Theorem 4.1. The Toeplitz matrix has coefficients $\eta = 0.15$, $\beta = 3.15$ and is of size 50×50 .

5. Numerical illustrations

In this section, we provide numerical evidence of the stability of the non-Hermitian skin effect and show how it competes with Anderson-type localisation of the eigenmodes in the bulk when the disorder is large. We will consider perturbations in both the geometry and the local values of the imaginary gauge potential. For the sake of brevity, we fix the size ℓ of the resonators and perturb independently either γ or the spacing s between the resonators.

5.1. Random perturbations of the geometry

We first consider systems of subwavelength resonators where the relative spacings are perturbed as

$$s_i = 1 + \varepsilon_i, \quad \varepsilon_i \sim \mathcal{U}_{[-\varepsilon, \varepsilon]}. \quad (5.1)$$

Here, $\mathcal{U}_{[-\varepsilon, \varepsilon]}$ is a uniform distribution with support in $[-\varepsilon, \varepsilon]$. In Figure 5.1a, we study how the eigenmodes of a system of 30 subwavelength resonators behave as the disorder increases. These results are averages based on 500 independent realisations. We show the relative proportion of eigenvalues that fall within the region of negative winding of the associated Toeplitz operator from Figure 2.2a, as well as the proportion of eigenmodes accumulating at the left edge (which for this and the following figures has been defined as the number of eigenvectors that attain their maximal value, in absolute terms, in one of the first two dimers). We consider values of the disorder strength that are small enough that the resonators are guaranteed to not overlap. Both these quantities are constant for small disorder strengths then decrease once the disorder strength passes a certain threshold (as predicted by Theorem 4.1). The intersection of these two sets is also shown.

One notices very similar trends in the three lines in Figure 5.1a, with small differences due to the imperfect formulation of the accumulation measure and the perturbations. On the other hand, Figure 5.1b shows the localisation of the eigenvectors for different disorder strengths. The localisation of the eigenvectors is measured using the quantity $\|v_i\|_\infty / \|v_i\|_2$ and the different lines correspond to different disorder strengths ε . We notice that the lines are indistinguishable, indicating that the localisation of the eigenvectors is independent of any random perturbation of the positions of the resonators.

Figure 5.1c shows similar stability properties as those in Figure 5.1a, but here the relative number of eigenvalues falling within the region with negative winding is plotted for different values of ε and γ . On the left side of the figure we see the topologically protected region: for these values of γ any small perturbation size ε will not cause any eigenvalue to exit the region and thus the corresponding eigenvector remains accumulated at the left edge of the structure.

The results in Figure 5.1 show how the proportion of eigenvectors localised to the left edge of the system decreases as the disorder increases. Studying in the eigenvectors themselves, as shown in Figure 5.2 for three different values of the disorder strength, we see that increasing disorder means an increasing number of eigenvectors are localised in the bulk rather than on the left edge. This behaviour is typical of Anderson-type localisation in disordered systems and demonstrates the internal competition between the skin effect and Anderson localisation.

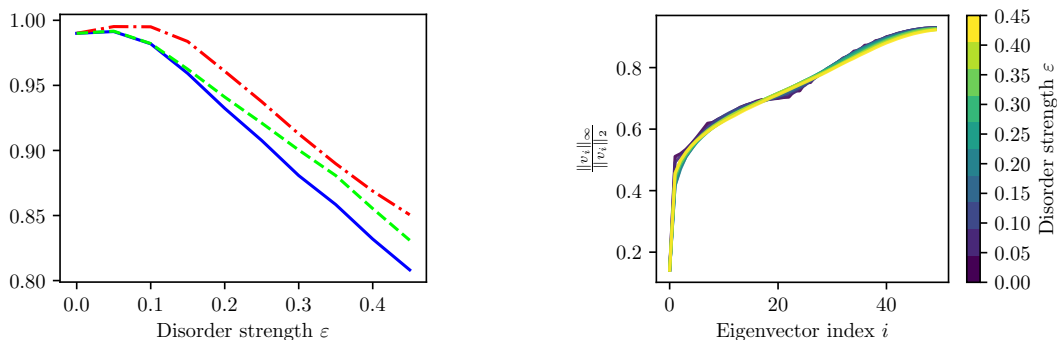
5.2. Random perturbations of the imaginary gauge potential

In this subsection we consider systems of subwavelength resonators where now the spacing between the resonators is fixed to $s_i = 1$, but the damping factor γ is allowed to be different in each resonator. Specifically, we consider

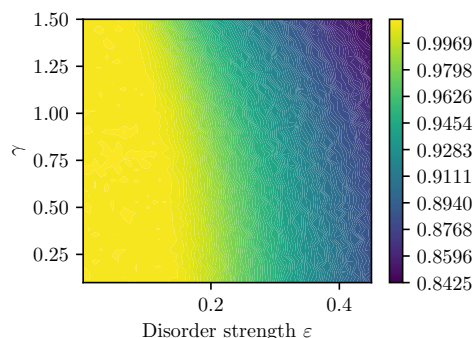
$$\gamma_i = 1 + \varepsilon_i, \quad \varepsilon_i \sim \mathcal{U}_{[-\varepsilon, \varepsilon]}, \quad (5.2)$$

where γ_i is the value taken by γ in the i -th resonator.

Figure 5.3 is the analogue of Figure 5.1 in this case. In this case, the disorder strength ε is allowed to vary over a larger range as we do not have the issue of resonators overlapping. Note however that large disorder, such as $|\varepsilon| > |\gamma| = 1$, will possibly induce different signs in the γ_i and thus striking changes in the coefficients of \mathcal{C}^γ . Figure 5.3a shows some similar



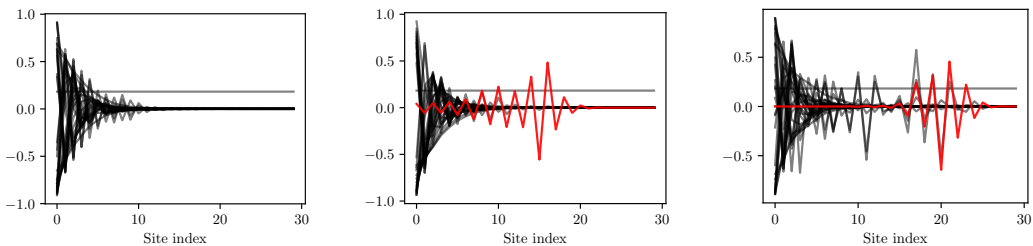
- (A) Eigenmode accumulation at one edge and topological winding. The green dashed line shows the average proportion of eigenvectors which are localised at the left edge. The red dash-dot line shows the average proportion of eigenvalues that lay in the topologically protected region. The blue solid line shows the proportion of eigenpairs that have *both* eigenvalues in the topologically protected region and eigenvectors accumulated on the left edge.
- (B) Eigenmode localisation. Each line shows the average eigenmode localisation for a different value of the disorder strength ε . For small ε the localisation is due to the skin effect, while for big ε it is consequence of the Anderson localisation. As the lines are indistinguishable we conclude that the eigenmode localisation is independent of disorder strength; as ε increases, modes might be localised in the bulk but will not become delocalised.



- (c) Phase change and topological protection. The color scale shows the average proportion of eigenvalues that lay in the topologically protected region for different values of γ . The left yellow zone is the stability region.

FIGURE 5.1. Competition between the non-Hermitian skin effect and Anderson localisation when perturbing the geometry. The non-Hermitian skin effect shows stability with respect to random perturbations. Outside of the stability region, there is competition with Anderson localisation. Averages are computed over 500 runs for a system of 50 resonators with $\ell = s = 1$.

behaviour to Figure 5.1a, in the sense that both quantities decrease as the disorder increases. However, for larger values of ε there is an obvious decoupling of the quantities. This is due to the fact that, for very large random perturbations, \widehat{C}^γ is very far from being Toeplitz and thus the symbol of the associated Toeplitz operator loses its meaning.



(A) Single realisation with disorder strength $\varepsilon = 0.1$. All eigenmodes are accumulated on the left edge. (B) Single realisation with disorder strength $\varepsilon = 0.2$. One eigenmode localised in the bulk is highlighted in red. (C) Single realisation with disorder strength $\varepsilon = 0.4$. One eigenmode localised in the bulk is highlighted in red.

FIGURE 5.2. Stability of the non-Hermitian skin effect under perturbations of the geometry. Eigenmode condensation on the left edge of the structure with some eigenmodes localised in the bulk. Single realisations with $N = 30$, $s = \ell = 1$, and $\varepsilon = 0.1, 0.2, 0.4$ for Figure 5.2a, 5.2b, and 5.2c respectively. This should be compared with Figure 2.2b, where there is no disorder.

On the other hand, Figure 5.3b shows the localisation measure of the eigenvectors for different disorder strengths. Eventhough the disorder is allowed to take much larger values here than in Figure 5.1b, we once again observe that the localisation of a given eigenvector is almost constant as the disorder changes.

Finally, Figure 5.3c shows the analogous results to Figure 5.1c. Once again, we see that there is a region of topological protection. This time, it is in the top-left of the diagram (for large space s and small disorder ε).

Figures 5.1 to 5.3 as a whole show an internal competition between the skin effect and the Anderson localisation: as disorder is introduced, modes transition from being condensed on the edge to being localised within the bulk.

5.3. Simultaneous perturbations of the geometry and the imaginary gauge potential

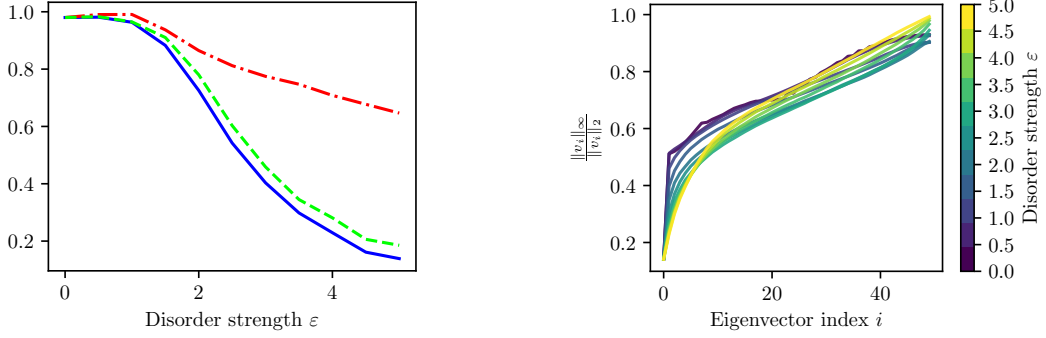
For the sake of completeness, in Figure 5.4 we present the result of perturbing γ and s simultaneously by

$$\begin{aligned} s_i &= 1 + \varepsilon_i, & \varepsilon_i &\sim \mathcal{U}_{[-\varepsilon_s, \varepsilon_s]} \\ \gamma_i &= 1 + \varepsilon_i, & \varepsilon_i &\sim \mathcal{U}_{[-\varepsilon_\gamma, \varepsilon_\gamma]}. \end{aligned}$$

The results show that the skin effect is very stable under any type of perturbations: the spacing between the resonators may be perturbed up to roughly 10% and simultaneously the γ factor up to 50% independently in every resonator and the accumulation of eigenmodes on one edge of the structure remains unaltered.

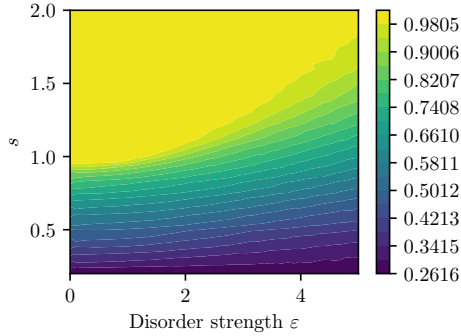
6. Concluding remarks

Based on a stability analysis of the eigenvalues and eigenvectors of the gauge capacitance matrix, we have proved robustness of the non-Hermitian skin effect with respect to random changes of the strength γ of the imaginary gauge potential and the spacing s between the resonators. We have also elucidated the topological origins of such robustness in our setting. Under random perturbations, the eigenmodes which remain localised at the edge of the structure are precisely those whose associated eigenvalues (which remain real valued) remain within the region of the complex plane corresponding to negative winding of the symbol of the corresponding Toeplitz operator. As the strength of the disorder increases, an increasing number of eigenmodes become localised in the bulk as their corresponding eigenfrequencies



(A) Eigenmode accumulation at one edge and topological winding. The green dashed line shows the average proportion of eigenvectors which are localised at the left edge. The red dash-dot line shows the the average proportion of eigenvalues that lay in the topologically protected region. The blue solid line shows the proportion of eigenpairs that have *both* eigenvalues in the topologically protected region and eigenvectors accumulated on the left edge.

(B) Eigenmode localisation. Each line shows the average eigenmode localisation for a different value of the disorder strength ε . For small ε the localisation is due to the skin effect, while for big ε it is consequence of the Anderson localisation. Thus, the localisation is much less sensitive to the perturbations than the accumulation (as the position of localisation may be away from the edge for large disorder).



(C) Phase change and topological protection. The color scale shows the average proportion of eigenvalues that lay in the topologically protected region for different values of s . The top-left yellow zone is the stability region.

FIGURE 5.3. Competition between the non-Hermitian skin effect and Anderson localisation when perturbing the complex gauge potential. The non-Hermitian skin effect is stable with respect to random perturbations. Outside of the stability region, there is a competition between the Non-Hermitian skin effect and the disorder-induced Anderson localisation. Averages 500 runs for a system of 50 resonators with $\ell = s = 1$.

leave the region of negative winding. This leads to a competition between the non-Hermitian skin effect and Anderson localisation in the bulk.

The results in this paper could be generalised to systems with periodically repeated cells of $K \geq 2$ resonators [6] and to higher dimensional systems, in which it is well known that

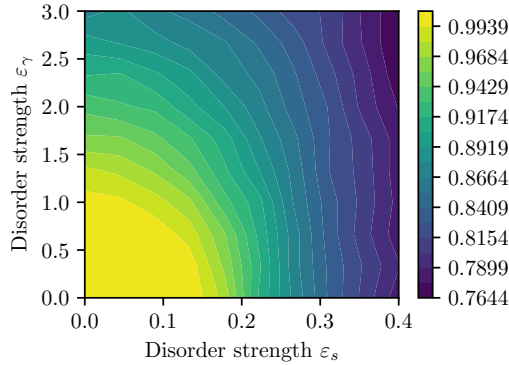


FIGURE 5.4. Phase transition for varying disorder strengths in γ and s . The color scale shows the average proportion of eigenvalues that lay in the topologically protected region for different values of ε_γ and ε_s . The bottom-left yellow zone is the stability region. The values are averages over 100 runs in a system of 50 resonators with $\ell = 1$.

the skin effect can be realised [2, 35]. Since our results are based on an asymptotic matrix model for subwavelength physics, they can also be generalised to analogous tight-binding models in condensed matter theory.

Acknowledgments

The work of PL was supported by Swiss National Science Foundation grant number 200021–200307. The work of BD was supported by a fellowship funded by the Engineering and Physical Sciences Research Council (EPSRC) under grant number EP/X027422/1.

Code availability

The software used to produce the numerical results in this work is openly available at <https://doi.org/10.5281/zenodo.8210678>.

References

- [1] AMMARI Habib, BARANDUN Silvio, CAO Jinghao, DAVIES Bryn and HILTUNEN Erik Orvehed, “Mathematical foundations of the non-Hermitian skin effect”, in: *arXiv preprint arXiv:2306.15587* (2023).
- [2] AMMARI Habib, BARANDUN Silvio, CAO Jinghao, DAVIES Bryn, HILTUNEN Erik Orvehed and LIU Ping, *The three-dimensional non-Hermitian Skin effect in systems of subwavelength resonators with imaginary gauge potential*, in preparation.
- [3] AMMARI Habib, BARANDUN Silvio and LIU Ping, “Perturbed Block Toeplitz matrices and the non-Hermitian skin effect in dimer systems of subwavelength resonators”, in: *arXiv preprint arXiv:2307.13551* (2023).
- [4] AMMARI Habib, DAVIES Bryn and HILTUNEN Erik Orvehed, “Anderson localization in the subwavelength regime”, in: *arXiv preprint arXiv:2205.13337* (2022).
- [5] AMMARI Habib, DAVIES Bryn and HILTUNEN Erik Orvehed, *Functional Analytic Methods for Discrete Approximations of Subwavelength Resonator Systems*, 2021, DOI: 10.48550/ARXIV.2106.12301.
- [6] AMMARI Habib, LI Bowen and ZOU Jun, “Mathematical Analysis of Electromagnetic Scattering by Dielectric Nanoparticles with High Refractive Indices”, in: *Transactions of the American Mathematical Society* 376.1 (2023), pp. 39–90.

- [7] ANDERSON Philip W, “Absence of diffusion in certain random lattices”, in: *Phys. Rev.* 109.5 (1958), p. 1492.
- [8] ASHIDAA Yuto, GONGA Zongping and UEDAA Masahito, “Non-Hermitian physics”, in: *Adv. Phys.* 69.3 (2020), pp. 249–435.
- [9] BRANDENBOURGER Martin, LOCSIN Xander, LERNER Edan and COULAIS Corentin, “Non-reciprocal robotic metamaterials”, in: *Nature Comm.* 10 (2019), p. 4608.
- [10] ELLIOTT Joseph Frederick, “The characteristic roots of certain real symmetric matrices”, in: (1953).
- [11] FRANCA S., KÖNYE V., HASSLER F., BRINK J. van den and FULGA C., “Non-Hermitian Physics without Gain or Loss: The Skin Effect of Reflected Waves”, in: *Phys. Rev. Lett.* 129 (2022), p. 086601.
- [12] GHATAK Ananya, BRANDENBOURGER Martin, VAN WEZEL Jasper and COULAIS Corentin, “Observation of Non-Hermitian Topology and Its Bulk–Edge Correspondence in an Active Mechanical Metamaterial”, in: *Proceedings of the National Academy of Sciences* 117.47 (2020), pp. 29561–29568.
- [13] GOLUB Gene H. and VAN LOAN Charles F., *Matrix computations*, Fourth, Johns Hopkins Studies in the Mathematical Sciences, Johns Hopkins University Press, Baltimore, MD, 2013.
- [14] GREGORY Robert T. and KARNEY David L., “A collection of matrices for testing computational algorithms”, in: (1969), pp. ix+154.
- [15] HATANO Naomichi and NELSON David R., “Localization Transitions in Non-Hermitian Quantum Mechanics”, in: *Physical Review Letters* 77.3 (July 1996), pp. 570–573, DOI: 10.1103/PhysRevLett.77.570.
- [16] HATANO Naomichi and NELSON David R., “Localization Transitions in Non-Hermitian Quantum Mechanics”, in: *Phys. Rev. Lett.* 77 (3 1996), pp. 570–573, DOI: 10.1103/PhysRevLett.77.570.
- [17] IPSEN Ilse CF and NADLER Boaz, “Refined perturbation bounds for eigenvalues of Hermitian and non-Hermitian matrices”, in: *SIAM Journal on Matrix Analysis and Applications* 31.1 (2009), pp. 40–53.
- [18] JIANG Hui, LANG Li-Jun, YANG Chao, ZHU Shi-Liang and CHEN Shu, “Interplay of non-Hermitian skin effects and Anderson localization in nonreciprocal quasiperiodic lattices”, in: *Phys. Rev. B* 100 (2019), p. 054301.
- [19] KAWABATA Kohei and SATO Masatoshi, “Real spectra in non-Hermitian topological insulators”, in: *Phys. Rev. Res.* 2 (2020), p. 033391.
- [20] LIN Quan, LI Tianyu, XIAO1 Lei, WANG Kunkun, YI Wei and XUE Peng, “Observation of non-Hermitian topological Anderson insulator in quantum dynamics”, in: *Nature Comm.* 13 (2022), p. 3229.
- [21] LONGHI S., GATTI D. and VALLE G.D., “Robust light transport in non-Hermitian photonic lattices”, in: *Scientific reports* 5 (2015), p. 13376, DOI: 10.1038/srep13376.
- [22] LONGHI Stefano, “Non-Hermitian skin effect beyond the tight-binding models”, in: *Phys. Rev. B* 104 (2021), p. 125109.
- [23] OKUMA Nobuyuki and SATO Masatoshi, “Non-Hermitian Topological Phenomena: A Review”, in: *Annu. Rev. Condens. Matter Phys.* 14 (2023), pp. 83–107.
- [24] PARLETT Beresford N, *The symmetric eigenvalue problem*, SIAM, 1998.
- [25] REIS DA SILVA RJ et al., *Matrix perturbations: bounding and computing eigenvalues*, OisterwijkUitgeverij BOXPress, 2011.
- [26] RIVERO Jose H. D., FENG Liang and GE Li, “Imaginary Gauge Transformation in Momentum Space and Dirac Exceptional Point”, in: *Physical Review Letters* 129.24 (Dec. 2022), p. 243901, DOI: 10.1103/PhysRevLett.129.243901.
- [27] SARKAR Ronika, HEGDE Suraj S. and NARAYAN Awadhesh, “Interplay of disorder and point-gap topology: Chiral modes, localization, and non-Hermitian Anderson skin effect in one dimension”, in: *Phys. Rev. B* 106 (2022), p. 014207.

REFERENCES

- [28] SJÖSTRAND Johannes and VOGEL Martin, “Large bidiagonal matrices and random perturbations”, in: *Journal of spectral theory* 6.4 (2016), pp. 977–1020.
- [29] SJÖSTRAND Johannes and VOGEL Martin, “Toeplitz band matrices with small random perturbations”, in: *Indagationes Mathematicae* 32.1 (2021), pp. 275–322.
- [30] WANG W., WANG X. and MA G., “Non-Hermitian morphing of topological modes”, in: *Nature* 608 (2022), pp. 50–55.
- [31] YOKOMIZO Kazuki, YODA Taiki and MURAKAMI Shuichi, “Non-Hermitian Waves in a Continuous Periodic Model and Application to Photonic Crystals”, in: *Phys. Rev. Res.* 4.2 (May 2022), p. 023089, DOI: 10.1103/PhysRevResearch.4.023089.
- [32] YOKOMIZO Kazuki, YODA Taiki and MURAKAMI Shuichi, “Non-Hermitian Waves in a Continuous Periodic Model and Application to Photonic Crystals”, in: *Phys. Rev. Res.* 4.2 (May 2022), p. 023089, DOI: 10.1103/PhysRevResearch.4.023089.
- [33] YUEH Wen-Chyuan, “Eigenvalues of several tridiagonal matrices.”, in: *Applied Mathematics E-Notes [electronic only]* 5 (2005), pp. 66–74.
- [34] YUEH Wen-Chyuan and CHENG Sui Sun, “Explicit eigenvalues and inverses of tridiagonal Toeplitz matrices with four perturbed corners”, in: *the ANZIAM Journal* 49.3 (2008), pp. 361–387.
- [35] ZHANG Kai, YANG Zhesen and FANG Chen, “Universal non-Hermitian skin effect in two and higher dimensions”, in: *Nature Commun.* 13 (2022), p. 2496.

HABIB AMMARI

ETH ZÜRICH, DEPARTMENT OF MATHEMATICS, RÄMISTRASSE 101, 8092 ZÜRICH, SWITZERLAND.

Email address: `habib.ammari@math.ethz.ch`

SILVIO BARANDUN

ETH ZÜRICH, DEPARTMENT OF MATHEMATICS, RÄMISTRASSE 101, 8092 ZÜRICH, SWITZERLAND.

Email address: `silvio.barandun@sam.math.ethz.ch`

BRYN DAVIES

DEPARTMENT OF MATHEMATICS, IMPERIAL COLLEGE LONDON, 180 QUEEN’S GATE, LONDON SW7 2AZ, UK.

Email address: `bryn.davies@imperial.ac.uk`

ERIK ORVEHED HILTUNEN

DEPARTMENT OF MATHEMATICS, YALE UNIVERSITY, 10 HILLHOUSE AVE, NEW HAVEN, CT 06511, USA.

Email address: `erik.hiltunen@yale.edu`

PING LIU

ETH ZÜRICH, DEPARTMENT OF MATHEMATICS, RÄMISTRASSE 101, 8092 ZÜRICH, SWITZERLAND.

Email address: `ping.liu@sam.math.ethz.ch`